

T-Mamba: Frequency-Enhanced Gated Long-Range Dependency

for Tooth 3D CBCT Segmentation

Jing Hao¹, Lei He¹, and Kuo Feng Hung^{2, *}

¹Huazhong University of Science and Technology, China

²The University of Hong Kong, China

*Corresponding author: hungkfg@hku.hk

Abstract

Efficient tooth segmentation in three-dimensional (3D) imaging, critical for orthodontic diagnosis, remains challenging due to noise, low contrast, and artifacts in CBCT images. Both convolutional Neural Networks (CNNs) and transformers have emerged as popular architectures for image segmentation. However, their efficacy in handling long-range dependencies is limited due to inherent locality or computational complexity. To address this issue, we propose T-Mamba, integrating shared positional encoding and frequency-based features into vision mamba, to address limitations in spatial position preservation and feature enhancement in frequency domain. Besides, we also design a gate selection unit to integrate two features in spatial domain and one feature in frequency domain adaptively. T-Mamba is the first work to introduce frequency-based features into vision mamba. Extensive experiments demonstrate that T-Mamba achieves new SOTA results on the public Tooth CBCT dataset and outperforms previous SOTA methods by a large margin, i.e., IoU + 3.63%, SO + 2.43%, DSC + 2.30%, HD -4.39mm, and ASSD -0.37mm. The code and models are publicly available at <https://github.com/isbrycee/T-Mamba>.

Keywords: Tooth CBCT Segmentation, Vision Mamba, Frequency Feature Modeling, Deep Learning.

1. Introduction

The evolutionary key of modern digital dentistry lies in the acquisition and segmentation of three-dimensional (3D) imaging. This technology finds several uses in oral and maxillofacial disciplines, including orthodontic diagnosis and treatment planning. Tooth segmentation, which consists of extracting a group of voxels from the 3D digital models with their intensity and density, is an essential phase in digital workflows. However, an accurate tooth segmentation process is challenging for several reasons. First of all, the 3D digital model is hard to observe due to the natural property of high noise and low contrast. In addition, the presence of metal fillings and prosthetic restorations in CBCT images introduces artifacts that induce distortions, significantly complicating the identification of teeth. Finally, CBCT is typically acquired in natural occlusion, posing challenges in distinguishing between lower and upper teeth due to their similar densities.

Deep learning has been widely used in the field of medical image segmentation, and many researchers are dedicated to employing deep learning techniques for automated segmentation of teeth in CBCT images Chen et al., 2023; Cui et al., 2019, 2021; Yin et al., 2023. CNNs and Transformers architecture have displayed considerable promise in medical image segmentation due to their ability to learn complex image features and provide accurate segmentation results. The CNNs can capture translational invariances and extract local features, and the Transformers excel at capturing global contextual information and improving the ability of long-range dependencies. Due to this complementary feature, many studies have explored incorporating Transformers into CNNs via hybrid network architectures. Nonetheless, the obvious shortcoming of Transformers is resource-intensive because the self-attention mechanism scales quadratically with the input size and poses challenges in terms of speed and memory usage with high-resolution biomedical images. While substantial effort has been dedicated to reducing the computational complexity of Transformers, they often come at the expense of sacrificing model accuracy Maaz et al., 2022; Zhai et al., 2023. Therefore, the efficient enhancement of long-range dependency in CNNs continues to be an unresolved issue.

Recently, motivated by the success of Mamba in language modeling, many studies have transferred this success from language to vision for the aim of achieving linear complexity without sacrificing global receptive fields Y. Liu et al., 2024; Zhu et al., 2024. However, we identify two limitations in utilizing vision mamba to assist CNNs for modeling long-range dependency. Firstly, CNNs can process 2D or 3D features directly while vision mamba structures is to handle 1D feature sequences. In the CNN and vision mamba hybrid architecture, the transformation of features by vision mamba inevitably leads to the loss of spatial position information. This spatial context is crucial, particularly in tasks requiring dense precise positional prediction. Secondly, due to the inherent imaging principles of medical images such as CT and X-ray, these images possess natural attributes of high noise and low contrast from a visual perspective. For such images, frequency domain-based feature representations are more accurate, unique, and robust. However, CNNs and vision mamba models typically extract semantic features solely from the spatial domain, overlooking the rich frequency domain-based information. As indicated by Azad et al., 2021, high-frequency components capture texture details, whereas low-frequency components encode shape information. Therefore, integrating frequency domain features with spatial domain representations holds promise for enhancing the image feature extraction in medical images, consequently improving the accuracy of prediction.

Inspired by these two limitations, we design a network named T-Mamba, which amalgamates our proposed Tim (Tooth Vision Mamba) block with DenseVNet Gibson et al., 2018 in multi-scale features, for Tooth CBCT image segmentation. The Tim block exhibits three key strengths: (1) It contains a shared bi-position embedding which are to compensate for the positional information lost during reshape operation. It is noteworthy that we employ a singular positional embedding within each feature-scale. This not only guarantees the preservation of spatial positions across feature maps of identical scales but reduces model parameters and computational burden. (2) It extracts image features in frequency domain thus we can derive more accurate, unique, and robust feature representations for medical images which are of high noise and low contrast. Based on the attributes of features at different scales, we have employed distinct bandpass filtering strategies tailored to each scale. (3) It includes a gate selection unit for integrating two features in spatial domain (both forward and backward directions) and one feature in frequency domain adaptively.

The gate selection unit is data-dependent and can assign weights for three distinctive features according to input sequence tokens.

Extensive experiments on Tooth CBCT segmentation task are conducted to verify the effectiveness of T-Mamba. Our T-Mamba outperforms previous state-of-the-art results on a public tooth CBCT dataset in a large margin, that is, IoU + 3.63%, SO + 2.43%, DSC +2.30%, HD -4.39mm, ASSD -0.37mm. Besides, we also implement ablation studies to verified the effectiveness of three components in our proposed Tim block. To the best of our knowledge, T-Mamba is the pioneering effort to incorporate frequency domain features into the vision mamba framework.

Our main contributions can be summarized as follows:

- We propose T-Mamba, which incorporates our designed Tim block with DenseVNet for global and local visual context modeling for Tooth CBCT segmentation.
- The Tim block is the first work to extract more robust and unique representations for medical images which are of high noise and low contrast by introducing frequency-based features.
- Without bells and whistles, T-Mamba achieves new SOTA results on the public Tooth CBCT dataset and outperforms previous SOTA methos in a large margin such as IoU + 3.63%, SO + 2.43%, DSC +2.30%, HD -4.39mm, ASSD -0.37mm.

2. Related Works

Vision mamba and its variants. Nguyen et al., 2022 is the first work applying SSMS into visual tasks and showing the potential that its performance may compete with ViT Dosovitskiy et al., 2020. Y. Liu et al., 2024 traverse the spatial domain and convert any non-causal visual image into order patch sequences. Zhu et al., 2024 marks the image sequences with position embeddings and compresses the visual representation with bidirectional SSMS. Yang et al., 2024 introduces the structured SSMS with spatiotemporal selective scan for medical video object segmentation task. Ma et al., 2024 which is a hybrid CNN-SSM architecture is proposed handle the long-range dependencies in biomedical image segmentation. In addition, there are some other works that leverage the SSMS into the medical image analysis field such as J. Liu et al., 2024; Ruan & Xiang, 2024; Xing et al., 2024; Ye & Chen, 2024.

3D Tooth CBCT Segmentation. Accurate and automatic depiction of individual teeth from CBCT images is a critical step to assist physicians in the diagnosis and treatment of oral diseases. Cui et al., 2019 was the first to use neural networks to achieve automatic tooth segmentation and identification from CBCT images. Cui et al., 2021 was designed for robust and efficient tooth segmentation on 3D dental scanned point cloud data. Jang et al., 2021 present a fully automated method of identifying and segmenting 3D individual teeth by hierarchical multi-step models. Chen et al., 2023 designed a U-shaped network which combines the advantages of CNN and Transformer for dental CBCT images segmentation. Yin et al., 2023 proposed a context-transformed architecture and obtained better performance in tooth CBCT segmentation.

2D Tooth X-Ray Segmentation. Accurate instance segmentation of teeth in panoramic dental X-rays is also another challenging task due to variations in tooth morphology and overlapping regions. Rubiu et al., 2023 utilized a mask region-based convolutional neural network (Mask-RCNN He et al., 2017) to segment tooth instances in Panoramic Dental X-ray. Silva et al.,

2020 brought a thorough study on tooth segmentation and numbering on panoramic X-ray images by means of end-to-end deep neural networks. Hou et al., 2023 proposed the Teeth U-Net by introducing context semantics and contrast enhancements upon U-Net. Haghanifar et al., 2023 proposed an automatic diagnosis system to detect dental caries in Panoramic images, using ensemble transfer learning and capsule classifier. Lin et al., 2023 designed a novel lightweight neural network scheme using knowledge distillation for dental X-ray image segmentation for the purpose of deployment on edge devices.

3. Methodology

3.1 Preliminaries for Mamba

The advanced state space models (SSM), i.e., structured state space sequence models (S4) and Mamba, are a type of systems that maps a 1-D continuous function or sequence $x(t) \in \mathbb{R} \mapsto y(t) \in \mathbb{R}$ through a hidden state $h(t) \in \mathbb{R}^N$. Mathematically, these models are typically formulated as linear ordinary differential equations (ODEs), as appears in (1):

$$\begin{aligned} h'(t) &= \mathbf{A}h(t) + \mathbf{B}x(t), \\ y(t) &= \mathbf{C}h(t), \end{aligned} \tag{1}$$

where the parameters include $\mathbf{A} \in \mathbb{R}^{N \times N}$ as the evolution parameter, and $\mathbf{B} \in \mathbb{R}^{N \times 1}$, $\mathbf{C} \in \mathbb{R}^{1 \times N}$ as the projection parameters.

The SSM-based models, as continuous-time models, should be discretized when integrated into deep learning algorithms. This discretization transformation is crucial to align the model with the sample rate of the underlying signal embodied in the input data [1]. Given the input $x(t) \in \mathbb{R}^{L \times D}$, a sampled vector within the signal flow of length L following [2], Equation (1) could be discretized as follows using the zeroth-order hold (ZOH) rule:

$$\begin{aligned} h_t &= \overline{\mathbf{A}}h_{t-1} + \overline{\mathbf{B}}x_t \\ y_t &= \overline{\mathbf{C}}h_t \\ \overline{\mathbf{A}} &= e^{\Delta \mathbf{A}} \\ \overline{\mathbf{B}} &= \Delta \mathbf{A}^{-1}(e^{\Delta \mathbf{A}} - \mathbf{I}) \cdot \Delta \mathbf{B} \\ \overline{\mathbf{C}} &= \mathbf{C}, \end{aligned} \tag{2}$$

where $\Delta \in \mathbb{R}^D$ is the timescale parameter.

Eventually, the models compute output y through a global convolution operation within a structured convolutional kernel $\overline{\mathbf{K}}$:

$$\begin{aligned} \overline{\mathbf{K}} &= (\overline{\mathbf{C}}\overline{\mathbf{B}}, \overline{\mathbf{C}}\overline{\mathbf{A}}\overline{\mathbf{B}}, \overline{\mathbf{C}}\overline{\mathbf{A}}^2\overline{\mathbf{B}}, \dots, \overline{\mathbf{C}}\overline{\mathbf{A}}^{L-1}\overline{\mathbf{B}}), \\ y &= \overline{\mathbf{K}} \otimes y_t. \end{aligned} \tag{3}$$

3.2 T-Mamba architecture

We enhance the representation modeling ability of CNN by leveraging Mamba’s linear scaling advantage and propose a general-purpose network T-Mamba for image segmentation. The architecture of the T-Mamba is sketched in Fig. 1, which amalgamates our proposed Tim block with

DenseVNet in multi-scale features. The T-Mamba consists of three feature scales and adopts the classical single-stage V-shaped architecture. We simply insert the Tim block after each CNN layer in DenseVNet to model the long-range dependency. T-Mamba can capture both localized fine-grained feature and long-range dependencies in terms of spatial domain and frequency domain. We hope it could open new avenues for efficient long-range dependency modeling in biomedical image analysis.

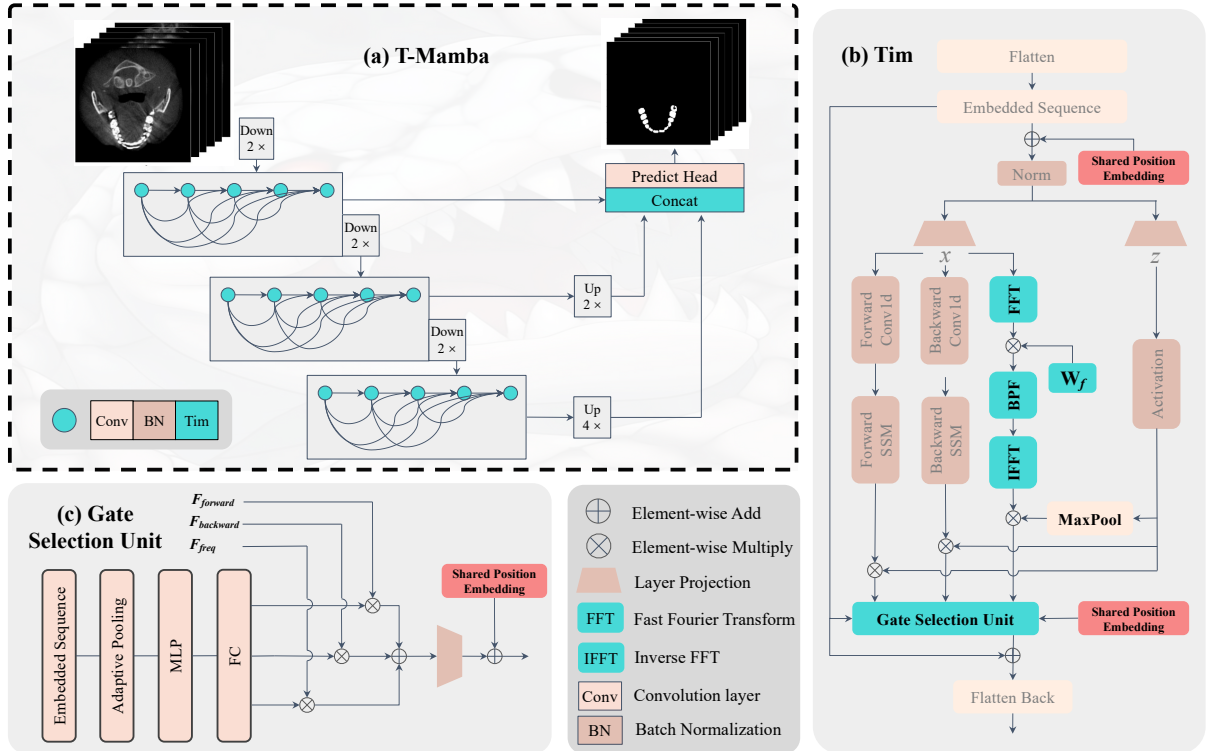


Figure 1: The framework of T-Mamba.

3.3 Tim block

The original Mamba block is devised for the 1-D sequence, which is not compatible for vision tasks requiring spatial-aware understanding. The Vision Mamba Zhu et al., 2024 proposed Vim block which incorporates the bidirectional sequence modeling upon the Mamba block. Based on this powerful design, we further enhance the vision feature modeling which is vital for 2D & 3D tooth segmentation tasks by introducing three components into the Vim block: 1) Shared bi-positional encoding compensation; 2) frequency-based band pass filtering; 3) Gated Selection unit. Our Tooth Vision Mamba (Tim) block is shown in Fig. 1.

Shared Dual Positional Encoding Compensation. Our T-Mamba network integrates the local feature extraction power of convolutional layers with the abilities of SSMs for capturing the long-range dependency. Convolutional layers typically handle 2-D or 3-D feature maps, while our designed Tim block focuses on process 1-D sequences. Consequently, reshaping high-dimensional features into 1-D feature tokens is essential. However, this process inevitably results in the loss of crucial positional information, vital for dense prediction tasks. To mitigate this, we employ a shared position embedding to compensate for the positional information lost during reshape operation.

Specifically, given an input feature with a shape of (B, C, H, W, D) , we first flattened it to

1-D feature tokens with a shape of (B, L, C) where $L = H \times W \times D$ and then add a learnable position embedding with a shape of (C, L) to feature tokens to retain positional information. Following [transformer is all u need], we initialize the position embedding via sinusoidal function:

$$\begin{aligned} PE_{(pos,2i)} &= \sin(pos/10000^{2i/d_{\text{model}}}), \\ PE_{(pos,2i+1)} &= \cos(pos/10000^{2i/d_{\text{model}}}), \end{aligned} \quad (4)$$

where pos is the position along with L and i is the index along with C. Regarding the output of Tim block, we also need to reshape the 1-D feature tokens into high-dimensional features for next convolutional operation. To further enhance the spatial information within the 1-D feature tokens, the positional embedding we used before is added to 1-D feature tokens again before reshaping them back into high-dimensional features. Note that we only use single positional embedding in each feature-scale. This practice ensures spatial positions remain unchanged in feature maps of the same scale, simultaneously reducing model parameters and computational burden. We posit that adding a shared dual positional embedding to both the input and output of the Tim block significantly preserves the positional information of high-dimensional features. Through ablation experiments, we validate that employing shared dual positional encoding leads to higher performance compared to using a single positional embedding.

Frequency-based band pass filtering. The Fourier domain plays a major role in extracting frequency-based analysis of image information and it’s evident that fine details and outlines could be captured in frequency domain even with poor quality X-ray Said et al., 2004; Y. Yu et al., 2021 and CT Azad et al., 2021; Li et al., 2024. The convolutional layers have a strong texture inductive bias, and they tend to learn texture-based feature. Representing an object in terms of frequency may reduce the effect of texture bias since only the high frequencies are responsible for the texture information (like boundaries) and lower frequencies might be related to the shape. Inspired by this, we evolve the structure of Vim by enhancing features extraction in frequency domain. Specifically, we firstly transform the sequence tokens X to the Fourier domain, then extract frequency features using learnable weight parameters and implement a bandpass filtering, and finally conduct the inverse Fourier transform to get the signal back. After that, the frequency feature is aggregated by the activated Z' with maxpooling operation. The whole process can be formulated as:

$$\begin{aligned} \mathcal{F}_{freq} &= IFFT(Bandpass(W_f(FFT(X)))) * Maxpool(Z'), \\ Bandpass &= \begin{cases} X * (|X| < S_{low}), X \in \text{low-level features}, \\ X * (S_{low} < |X| < S_{high}), X \in \text{medium-level features}, \\ X * (|X| > S_{high}), X \in \text{high-level features}, \end{cases} \end{aligned} \quad (5)$$

where S_{low} , S_{high} are the thresholds of bandpass filtering. In our experiments, we set $S_{low}=0.1$ and $S_{high} = 0.9$. The low-level, medium-level, high-level indicates three different feature scales in our network, respectively.

Gate Selection Unit. The evolved Vim block consists of two features in spatial domain (both forward and backward directions) and one feature in frequency domain. We devise a Gate Selection Unit with the objective of fusing these distinctive features adaptively. The input embedding sequence is firstly down-sampled to a fixed dimension such as 2048, and it is projected through MLP (Multi linear projection), along with a fully connection to predict three proportions

corresponding to three features. After that, the f_{fuse} is derived by weighted summation of three features and then projected by a linear layer, and Gate Selection Unit outputs the sum of the f_{fuse} , the residual information, and the shared position embedding.

$$\begin{aligned}
S_{forward}, S_{backward}, S_{freq} &= FC(MLP(Adaptive Pooling(X))), \\
f_{fuse} &= (S_{forward} * F_{forward} + S_{backward} * F_{backward} + S_{freq} * F_{freq}), \\
O_{gate} &= f_{fuse} + X + shared pos,
\end{aligned} \tag{6}$$

where shared pos is the shared position embedding mentioned earlier. The Gate Selection Unit is data-dependent because the three weight coefficients are computed from source X, and these weight coefficients are then used to update different forms of features of X. Consequently, the Gate Selection Unit can adaptively adjust the combination of the three forms of features based on different inputs, thus obtaining a better feature representation.

4. Experiments and Discussion

We conduct extensive comparisons with a range of stage-of-the-art (SOTA) methods and numerous vision mamba variants, demonstrating the superiority of our T-Mamba and achieving new stage-of-the-art results. Besides, we also did ablation study on each component in Tim block.

4.1 Experiment Settings

4.1.1 3D CBCT Dataset

The 3D CBCT dataset used in our study is collected from a large-scale CBCT dataset released by Cui et al., 2022. This large-scale dataset is used for segmentation and reconstruction of individual teeth and alveolar bone, and it consists of 4938 CBCT scans from 15 different centers in China with varying data distributions. However, only partial data has been released due to the privacy issues and regulation policies in hospitals. The data setting in our study is identical with Zhong et al., 2024, which 129 scans are used in total, dividing into a training set of 103 scans and a test set of 26 scans. The physical resolution of these scans is isotropic resolution, varying from 0.2 to 0.4 mm^3 . Some samples are showed in Figure 2.

4.1.2 Implementation Details

All experiments are conducted using pyTorch on one NVIDIA V100 GPU 32G. The image pre-processing and data augmentation is strictly the same as Zhong et al., 2024. For the 3D CBCT tooth dataset, we resample each 3D image to a uniform voxel spacing of $0.5 \times 0.5 \times 0.5mm$ and then randomly crop every image to $160 \times 160 \times 96$ size for model inputs. The training process incorporates the AdamW optimizer with betas set to (0.9, 0.999), a momentum of 0.8, a ReduceLROnPlateau learning rate scheduler, an initial learning rate of $5e-3$, and a weight decay of $5e-5$. Following the configuration in Zhong et al., 2024, T-Mamba undergo training from scratch for 20 epochs. Five evaluation metrics were employed to assess the network’s performance, including Dice Similarity Coefficient (DSC), Intersection over Union (IoU), Mean Intersection over Union (mIoU), Accuracy (ACC), Hausdorff Distance (HD), Average Symmetric Surface Distance (ASSD), and Surface Overlap (SO).

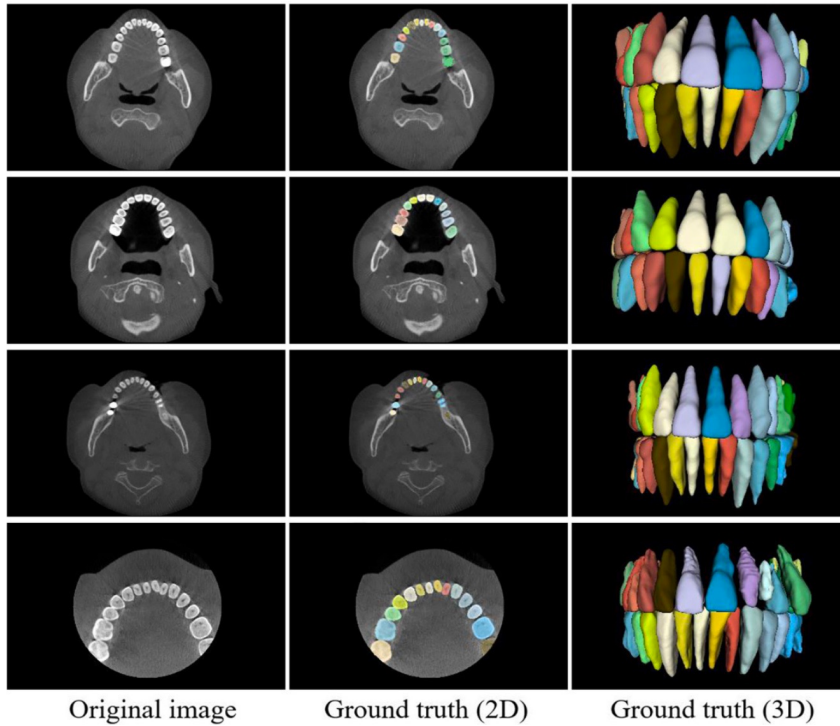


Figure 2: The 3D CBCT tooth dataset samples.

4.2 Quantitative Comparisons

Table 1: Comparison results of different methods on the 3D CBCT tooth dataset. The best results are in bold. \uparrow means higher values are better, \downarrow means lower values are better. Most scores of competing methods are taken from PMFSNet3D.

Method	FLOPs(G) \downarrow	Params(M) \downarrow	HD(mm) \downarrow	ASSD(mm) \downarrow	IoU(%) \uparrow	SO(%) \uparrow	DSC(%) \uparrow
UNet3D Çiçek et al., 2016	2223.03	16.32	113.79	22.40	70.62	70.72	36.67
DenseVNet Gibson et al., 2018	23.73	0.87	8.21	1.14	84.57	94.88	91.15
AttentionUNet3D Oktay et al., 1804	2720.79	94.48	147.10	61.10	52.52	42.49	64.08
DenseVoxelNet L. Yu et al., 2017	402.32	1.78	41.18	3.88	81.51	92.50	89.58
MultiResUNet3D Ibtihaz, 2019	1505.38	17.93	74.06	8.17	76.19	81.70	65.45
UNETR Hatamizadeh et al., 2022	229.19	93.08	107.89	17.95	74.30	73.14	81.84
SwinUNETR Hatamizadeh et al., 2021	912.35	62.19	82.71	7.50	83.10	86.80	89.74
TransBTS Wenxuan et al., 2021	306.80	33.15	29.03	4.10	82.94	90.68	39.32
nnFormer Zhou et al., 2023	583.49	149.25	51.28	5.08	83.54	90.89	90.66
3D UX-Net Lee et al., 2022	1754.79	53.01	108.52	19.69	75.40	73.48	84.89
PMFSNet3D Zhong et al., 2024	15.14	0.63	5.57	0.79	84.68	95.10	91.30
T-Mamba (Ours)	-	-	1.18	0.42	88.31	97.53	93.60
	-	-	-4.39	-0.37	+3.63	+2.43	+2.30

To evaluate the performance of our T-Mamba on a 3D CBCT tooth dataset, we comprehensively compare it with several state-of-the-art (SOTA) 3D networks spanning a range of neural network architectures. These networks includes the UNet3D and its variants (MultiResUNet3D, AttentionUNet3D and PMFSNet3D), the DenseVNet and its variants (DenseVoxelNet), the transformer-based networks like UNETR, SwinUNETR, TransBTS, nnFormer, and 3D UX-Net. Table 2 demonstrates the comparisons in terms of the computational complexity and effectiveness. Overall, T-Mamba achieves the best results in all metrics compared to current state-of-the-art methods and it outperforms the SOTA method PMFSNet3D from accuracy perspectives by a large margin. More specifically, T-Mamba reduces the Hausdorff Distance (HD)

by **4.39 mm** and the Average Symmetric Surface Distance (ASSD) by **0.37 mm**. Additionally, T-Mamba enhances the Intersection over Union (IoU) by **3.63%**, the Similarity Overlap (SO) by **2.43%**, and the Dice Similarity Coefficient (DSC) by **2.30%**.

4.3 Ablation study

We conduct experiments to show the effectiveness of our proposed components in Tim block by adding them one at a time. First and foremost, we directly add vanilla Vim block into DenseVNet for introducing the global feature relationship modeling with linear complexity. The metric IoU, SO, DSC improve by 2.79%, 0.93%, 1.89%, respectively; but the metric HD and ASSD increase 1.32 and 0.11mm, respectively. This phenomenon indicates that the Vim block which could capture the long-range dependency from image features is beneficial to tooth CBCT segmentation while still exists some shortcomings. To further enhance the performance of Vim block, we introduce three components: 1) Shared bi-positional encoding compensation; 2) frequency-based bandpass filtering; 3) Gated Selection unit.

Regarding the positional encoding compensation, all metrics except HD get worse when only using the pre-position embedding which is inserted before norm operation in Tim block. On the other hand, only the metric ASSD and SO are improved when utilizing the post-position embedding which is inserted in gate selection unit. To our surprised, the shared bi-position embedding could bring significant improvements in all metrics, especially for HD and ASSD metrics. These three experiments show that the shared bi-position encoding is crucial for compensating the loss of positional information during the reshape operations of input and output, and can improve segmentation accuracy without introducing extra model parameters. After that, we add the residual connection from input sequence to output sequence, and this step can bring slight increases in all metrics. We also leverage the frequency-based bandpass filtering to extract the distinctive feature representation in the frequency domain. There is a small rise in the metric IoU and DSC. Ultimately, the gate selection unit is added to fuse three kinds of features and this unit dramatically increase the metric IoU, SO, DSC. In a word, our proposed Tim block enhances the metrics IoU, SO, DSC by 3.74%, 2.65%, 2.45%, respectively, and reduces the metrics HD and ASSD by 7.03mm and 0.72mm, respectively, compared with DenseVNet baseline. Besides, our Tim block achieves higher results compared with Vim block.

Table 2: The ablation study of our Tim block. \uparrow means higher values are better, \downarrow means lower values are better.

Method	HD(mm) \downarrow	ASSD(mm) \downarrow	IoU(%) \uparrow	SO(%) \uparrow	DSC(%) \uparrow
DenseVNet	8.21	1.14	84.57	94.88	91.15
+ Vim	9.53	1.25	87.36	95.81	93.04
+ Pre Pos	7.89	1.79	87.00	95.35	92.80
+ Post Pos	10.65	1.00	87.10	96.23	92.87
+ Shared bi-Pos	1.22	0.59	87.65	96.79	93.20
+ Residual Connection	1.10	0.39	87.95	97.48	93.40
+ FFT Bandpass Filtering	1.18	0.67	88.05	97.26	93.47
+ Gate Selection Unit	1.18	0.42	88.31	97.53	93.60

5. Conclusion

We have proposed T-Mamba to achieve global and local visual context modeling for Tooth CBCT segmentation. Thanks to the proposed Tim block that integrates shared positional encoding and frequency-based features into vision mamba, we address limitations in spatial position preservation and feature enhancement in frequency domain for medical images which are of high noise and low contrast. Extensive experiments demonstrate that T-Mamba achieves new SOTA results on the public Tooth CBCT dataset, showing that Tim has great potential to be the next-generation feature extractor for efficient long-range dependency modeling in biomedical image analysis.

In future works, we endeavor to explore the self-supervised learning, such as mask image modeling pretraining, in conjunction with our proposed Tim block for tooth CBCT and X-Ray segmentation tasks. We anticipate that this advancement in technology will further propel the evolution of modern digital dentistry.

References

- Azad, R., Bozorgpour, A., Asadi-Aghbolaghi, M., Merhof, D., & Escalera, S. (2021). Deep frequency re-calibration u-net for medical image segmentation. *Proceedings of the IEEE/CVF International Conference on Computer Vision*, 3274–3283.
- Chen, Z., Chen, S., & Hu, F. (2023). Cta-unet: Cnn-transformer architecture unet for dental cbct images segmentation. *Physics in Medicine & Biology*, 68(17), 175042.
- Çiçek, Ö., Abdulkadir, A., Lienkamp, S. S., Brox, T., & Ronneberger, O. (2016). 3d u-net: Learning dense volumetric segmentation from sparse annotation. *Medical Image Computing and Computer-Assisted Intervention—MICCAI 2016: 19th International Conference, Athens, Greece, October 17–21, 2016, Proceedings, Part II 19*, 424–432.
- Cui, Z., Fang, Y., Mei, L., Zhang, B., Yu, B., Liu, J., Jiang, C., Sun, Y., Ma, L., Huang, J., et al. (2022). A fully automatic ai system for tooth and alveolar bone segmentation from cone-beam ct images. *Nature communications*, 13(1), 2096.
- Cui, Z., Li, C., Chen, N., Wei, G., Chen, R., Zhou, Y., Shen, D., & Wang, W. (2021). Tsegnet: An efficient and accurate tooth segmentation network on 3d dental model. *Medical Image Analysis*, 69, 101949.
- Cui, Z., Li, C., & Wang, W. (2019). Toothnet: Automatic tooth instance segmentation and identification from cone beam ct images. *Proceedings of the IEEE/CVF conference on computer vision and pattern recognition*, 6368–6377.
- Dosovitskiy, A., Beyer, L., Kolesnikov, A., Weissenborn, D., Zhai, X., Unterthiner, T., Dehghani, M., Minderer, M., Heigold, G., Gelly, S., et al. (2020). An image is worth 16x16 words: Transformers for image recognition at scale. *arXiv preprint arXiv:2010.11929*.
- Gibson, E., Giganti, F., Hu, Y., Bonmati, E., Bandula, S., Gurusamy, K., Davidson, B., Pereira, S. P., Clarkson, M. J., & Barratt, D. C. (2018). Automatic multi-organ segmentation on abdominal ct with dense v-networks. *IEEE transactions on medical imaging*, 37(8), 1822–1834.
- Haghanifar, A., Majdabadi, M. M., Haghanifar, S., Choi, Y., & Ko, S.-B. (2023). Paxnet: Tooth segmentation and dental caries detection in panoramic x-ray using ensemble transfer learning and capsule classifier. *Multimedia Tools and Applications*, 82(18), 27659–27679.

- Hatamizadeh, A., Nath, V., Tang, Y., Yang, D., Roth, H. R., & Xu, D. (2021). Swin unetr: Swin transformers for semantic segmentation of brain tumors in mri images. *International MICCAI Brainlesion Workshop*, 272–284.
- Hatamizadeh, A., Tang, Y., Nath, V., Yang, D., Myronenko, A., Landman, B., Roth, H. R., & Xu, D. (2022). Unetr: Transformers for 3d medical image segmentation. *Proceedings of the IEEE/CVF winter conference on applications of computer vision*, 574–584.
- He, K., Gkioxari, G., Dollár, P., & Girshick, R. (2017). Mask r-cnn. *Proceedings of the IEEE international conference on computer vision*, 2961–2969.
- Hou, S., Zhou, T., Liu, Y., Dang, P., Lu, H., & Shi, H. (2023). Teeth u-net: A segmentation model of dental panoramic x-ray images for context semantics and contrast enhancement. *Computers in Biology and Medicine*, 152, 106296.
- Ibtehaz, M. M., Nabil. (2019). Rethinking the u-net architecture for multimodal biomedical image segmentation. *arXiv*.
- Jang, T. J., Kim, K. C., Cho, H. C., & Seo, J. K. (2021). A fully automated method for 3d individual tooth identification and segmentation in dental cbct. *IEEE transactions on pattern analysis and machine intelligence*, 44(10), 6562–6568.
- Lee, H. H., Bao, S., Huo, Y., & Landman, B. A. (2022). 3d ux-net: A large kernel volumetric convnet modernizing hierarchical transformer for medical image segmentation. *arXiv preprint arXiv:2209.15076*.
- Li, L., Liu, Q., Shi, X., Wei, Y., Li, H., & Xiao, H. (2024). Ucfiltersnet: Cross-filtering transformer-based network for ct image segmentation. *Expert Systems with Applications*, 238, 121717.
- Lin, S., Hao, X., Liu, Y., Yan, D., Liu, J., & Zhong, M. (2023). Lightweight deep learning methods for panoramic dental x-ray image segmentation. *Neural Computing and Applications*, 35(11), 8295–8306.
- Liu, J., Yang, H., Zhou, H.-Y., Xi, Y., Yu, L., Yu, Y., Liang, Y., Shi, G., Zhang, S., Zheng, H., et al. (2024). Swin-umamba: Mamba-based unet with imagenet-based pretraining. *arXiv preprint arXiv:2402.03302*.
- Liu, Y., Tian, Y., Zhao, Y., Yu, H., Xie, L., Wang, Y., Ye, Q., & Liu, Y. (2024). Vmamba: Visual state space model. *arXiv preprint arXiv:2401.10166*.
- Ma, J., Li, F., & Wang, B. (2024). U-mamba: Enhancing long-range dependency for biomedical image segmentation. *arXiv preprint arXiv:2401.04722*.
- Maaz, M., Shaker, A., Cholakkal, H., Khan, S., Zamir, S. W., Anwer, R. M., & Shahbaz Khan, F. (2022). Edgenext: Efficiently amalgamated cnn-transformer architecture for mobile vision applications. *European Conference on Computer Vision*, 3–20.
- Nguyen, E., Goel, K., Gu, A., Downs, G., Shah, P., Dao, T., Baccus, S., & Ré, C. (2022). S4nd: Modeling images and videos as multidimensional signals with state spaces. *Advances in neural information processing systems*, 35, 2846–2861.
- Oktay, O., Schlemper, J., Folgoc, L. L., Lee, M., Heinrich, M., Misawa, K., Mori, K., McDonagh, S., Hammerla, N. Y., Kainz, B., et al. (2018). Attention u-net: Learning where to look for the pancreas. *arXiv preprint arXiv:1804.03999*.
- Ruan, J., & Xiang, S. (2024). Vm-unet: Vision mamba unet for medical image segmentation. *arXiv preprint arXiv:2402.02491*.

- Rubiu, G., Bologna, M., Cellina, M., Cè, M., Sala, D., Pagani, R., Mattavelli, E., Fazzini, D., Ibba, S., Papa, S., et al. (2023). Teeth segmentation in panoramic dental x-ray using mask regional convolutional neural network. *Applied Sciences*, 13(13), 7947.
- Said, E., Fahmy, G. F., Nassar, D., & Ammar, H. (2004). Dental x-ray image segmentation. *Biometric Technology for Human Identification*, 5404, 409–417.
- Silva, B., Pinheiro, L., Oliveira, L., & Pithon, M. (2020). A study on tooth segmentation and numbering using end-to-end deep neural networks. *2020 33rd SIBGRAPI conference on graphics, patterns and images (SIBGRAPI)*, 164–171.
- Wenxuan, W., Chen, C., Meng, D., Hong, Y., Sen, Z., & Jiangyun, L. (2021). Transbts: Multimodal brain tumor segmentation using transformer. *International Conference on Medical Image Computing and Computer-Assisted Intervention, Springer*, 109–119.
- Xing, Z., Ye, T., Yang, Y., Liu, G., & Zhu, L. (2024). Segmamba: Long-range sequential modeling mamba for 3d medical image segmentation. *arXiv preprint arXiv:2401.13560*.
- Yang, Y., Xing, Z., & Zhu, L. (2024). Vivim: A video vision mamba for medical video object segmentation. *arXiv preprint arXiv:2401.14168*.
- Ye, Z., & Chen, T. (2024). P-mamba: Marrying perona malik diffusion with mamba for efficient pediatric echocardiographic left ventricular segmentation. *arXiv preprint arXiv:2402.08506*.
- Yin, Y., Xu, W., Chen, L., & Wu, H. (2023). Cot-unet++: A medical image segmentation method based on contextual transformer and dense connection. *Mathematical Biosciences and Engineering*, 20(5), 8320–8336.
- Yu, L., Cheng, J.-Z., Dou, Q., Yang, X., Chen, H., Qin, J., & Heng, P.-A. (2017). Automatic 3d cardiovascular mr segmentation with densely-connected volumetric convnets. *Medical Image Computing and Computer-Assisted Intervention- MICCAI 2017: 20th International Conference, Quebec City, QC, Canada, September 11-13, 2017, Proceedings, Part II 20*, 287–295.
- Yu, Y., She, K., & Liu, J. (2021). Wavelet frequency separation attention network for chest x-ray image super-resolution. *Micromachines*, 12(11), 1418.
- Zhai, Y., Hao, J., Gao, L., Li, X., Gao, Y., & Han, S. (2023). Simple parameter-free self-attention approximation. *arXiv preprint arXiv:2307.12018*.
- Zhong, J., Tian, W., Xie, Y., Liu, Z., Ou, J., Tian, T., & Zhang, L. (2024). Pmfsnet: Polarized multi-scale feature self-attention network for lightweight medical image segmentation. *arXiv preprint arXiv:2401.07579*.
- Zhou, H.-Y., Guo, J., Zhang, Y., Han, X., Yu, L., Wang, L., & Yu, Y. (2023). Nnformer: Volumetric medical image segmentation via a 3d transformer. *IEEE Transactions on Image Processing*.
- Zhu, L., Liao, B., Zhang, Q., Wang, X., Liu, W., & Wang, X. (2024). Vision mamba: Efficient visual representation learning with bidirectional state space model. *arXiv preprint arXiv:2401.09417*.